An Energy-Efficient Optical Wireless OFDMA Scheme for Medical Body-Area Networks

Md. Jahid Hasan, *Member, IEEE*, Mohammad Ali Khalighi, *Senior Member, IEEE*,
Volker Jungnickel, *Member, IEEE*, Luis Nero Alves, *Member, IEEE*,
and Bastien Béchadergue

Abstract—The transfer of health monitoring data from multiple patients using wireless body-area networks requires the use of robust, and energy and bandwidth efficient multiple-access schemes. This paper considers the frequency-division multiple access for the wireless uplink to a fixed access point when using infrared signals to collect medical data from several patients inside an emergency waiting room. The conventional optical orthogonal scheme applies Hermitian symmetry to obtain real-valued signals, which implies increased computational complexity. We consider a new approach transmitting only the real part of a complex-valued signal, where no such constraint is imposed. Based on the proposed scheme, and taking into account the limited dynamic range of an infrared light-emitting diode, we study the performance of direct current biased and asymmetrically clipped schemes, and show their advantage in terms of energy efficiency and computational complexity, as compared with the conventional schemes. For instance, we show that by using asymmetric clipping, around $35\,\text{mW}$ less transmit power is needed to achieve a bit error rate of 10^{-3} in the considered scenario. We also demonstrate the robustness of the proposed scheme against multiple access interference.

Index Terms—Wireless body area networks, energy efficiency, optical wireless communications, multiple access, OFDMA.

Md. Jahid Hasan was with the Aix-Marseille University, CNRS, Centrale Marseille, Institut Fresnel, Marseille, France, and also with Oledcomm SAS, 78140 Vélizy-Villacoublay, France. He is now with the Department of Electrical and Electronic Engineering, American International University-Bangladesh, Dhaka 1229, Bangladesh (e-mail: jahid.hasan@aiub.edu).

Mohammad Ali Khalighi is with the Aix-Marseille University, CNRS, Centrale Marseille, Institut Fresnel, Marseille, France (e-mail: ali.khalighi@fresnel.fr).

Volker Jungnickel is with the Fraunhofer-Institut für Nachrichtentechnik, Heinrich-Hertz-Institut, 10587 Berlin, Germany (e-mail: volker.jungnickel@hhi.fraunhofer.de).

Luis Nero Alves is with the Instituto de Telecomunicações and the Departamento de Electrónica, Telecomunicações e Informática, Universidade de Aveiro, 3810-193 Aveiro, Portugal (e-mail: nero@ua.pt).

Bastien Béchadergue is with the Laboratoire d'Ingénierie des Systèmes de Versailles, Université de Versailles Saint-Quentin, Université Paris-Saclay, 78140 Vélizy-Villacoublay, France (e-mail: bastien.bechadergue@uvsq.fr).

Digital Object Identifier 10.1109/TGCN.2022.3161413

I. Introduction

THE DELAY in adequate treatment or hospitalization, due to the long waiting times in an emergency reception room, is the leading cause of patient mortality in hospitals [1]. This situation can be improved by identifying any deterioration of patients health conditions at an early stage. Continuous real-time monitoring of patients inside the emergency waiting room is crucial for a rapid intervention in order to minimize severe medical complications. This can be achieved by sending timely data from the health monitoring sensors, through the use of wireless body area networks (WBANs) to a central computer which causes an alarm if needed [2], [3], [4]. In a WBAN, from a data transmission perspective, at first, all on-body sensors send the medical data to a coordinator node (CN), placed on the body, which is referred to as intra-WBAN communications. Then, the CN transmits these collected data to an off-body network via an access point (AP), which is called extra-WBAN communication [5], [6].

A. OWC-Based WBAN

Optical wireless communications (OWC) based on visible light (VL) and infrared (IR) are considered as one of key enabling technologies for the future networks, in particular, in medical applications [7], [8]. This is, in particular, due to their energy efficiency, immunity to electromagnetic interference, and availability of unlicensed spectrum, as compared to radio-frequency (RF) solutions. In addition, in an OWC-based WBAN, the inherent immunity against eavesdropping on confidential health information (due to the confinement of light in indoor scenarios) enhances the security features [9].

In this paper, we consider the use of IR links for the uplink extra-WBANs, where a CN placed on the patient body transmits the medical data to an AP in an emergency waiting room scenario. The use of IR rather than VL is to avoid user discomfort and visual annoyance [6]. VL can eventually be used in the downlink, i.e., from the AP to the CN, by using the light-emitting diode (LED) based luminaries; this way, the interference between the uplink and downlink can also be avoided [10]. Concerning the IR uplink, one major concern is eye-safety, which imposes a limitation on the transmitted optical power according to the IEC (International Electro-technical Commission) standard [11]. Fortunately, LEDs typically emit a wide beam from a large area, enabling the use of relatively high optical powers and link ranges of a few meters.

B. Need for Efficient Multiple Access Solution

In practice, in a typical emergency waiting room scenario, a large number of patients may need to be monitored simultaneously. This should be managed by using an efficient multiple access (MA) solution that allows several patients to share the same communication channel for the transfer of their medical data. Considering a few number of patients inside a hospital ward, orthogonal multiple access (OMA) schemes such as time- and code-division MA (TDMA and CDMA) were proposed for WBANs in [6], [12], [13], [14], [15], [16] because of their relatively low implementation complexity. However, their complexity increases with increased number of users due to the increasing synchronization requirements for TDMA and the longer signatures for CDMA. The increased number of users also results in reduced per-user data-rate. To address these issues, non-orthogonal multiple access (NOMA) have been considered, such as a bandwidth (BW) efficient sparse code NOMA technique that was proposed for health information monitoring in [17]. However, code-domain NOMA techniques generally suffer from high decoding complexity, in particular, with increased number of users [18]. Alternatively, power-domain NOMA can be used [19] but in addition to the high computational complexity of successive interference cancellation (SIC) detection [20], [21] for large numbers of users, the performance is highly affected by the correlation between the users' channels [22]. This is usually the case in our considered application due to closely placed patients inside the emergency waiting room and their mobility.

C. Frequency Division Optical Multiple Access

Optical orthogonal frequency-division multiplexing (O-OFDM) is quite efficient for addressing frequency selectivity of the aggregate channel (due to BW limited channel, transmitter (Tx), and/or receiver (Rx)) [23], [24]. Considering intensity modulation with direct detection (IM/DD), to obtain a real-valued "time-domain" (TD) signal in O-OFDM, Hermitian symmetry (HS) is usually imposed on the transmitted "frequency domain" (FD) signal frame. Due to the constraint of signal positivity, before modulating the LED, a DC-bias is further added to the signal before lower clipping; what is usually called direct current offset (DC) O-OFDM. Alternatively, asymmetrically clipped (AC) O-OFDM can be used, which modulates only the odd sub-carriers and zero-clips the negative TD signal afterwards [25], resulting in a spectral efficiency loss of factor 2, compared to DCO-OFDM [26].

One main issue with O-OFDM is the relatively high peak-to-average-power ratio (PAPR) of the modulated signal given the limited dynamic range (DR) of the optical front-ends [27], [28], [29]. Although a high PAPR does not affect the thermal limitations of the LED in the case of relatively fast signal modulation considered here [30], in order to avoid the need to low power-efficiency power amplifiers, the PAPR is further limited by further upper clipping the transmit signal. The resulting signal distortion due to lower and upper clipping is usually modeled by considering the so-called clipping noise [31]. Countless solutions have been proposed so far to reduce the PAPR of an O-OFDM signal, e.g., based on block coding, selective mapping, and pilot assisted transmission, usually at the cost of increased complexity [32], [33].

The extension of O-OFDM to O-OFDMA is known as an efficient MA technique [34] that we consider here in order to satisfy the demand for large transmission BW (due to a relatively large number of users) and to manage the MA interference (MAI). Considering battery-powered CNs, power consumption is crucial, which is related to the computational complexity and the transmit optical power. An alternative approach to O-OFDMA is TDMA scheduling of O-OFDM, which offers a better energy efficiency at the cost of reduced performance [35]. However, due to the low sensing rate of the medical sensors (the corresponding duty cycle can be as low as typically 1% [3]), TDMA based schemes impose additional complexity with the increased number of users. Another alternative is the so-called optical single-carrier FDMA (O-SCFDMA) [36]. SCFDMA has been adopted in the LTE standard as the uplink MA scheme due to its lower PAPR [37], [38]. Compared to OFDMA, additional discrete Fourier transform (DFT) pre-coding is required at the Tx side when using SCFDMA, as well as some additional filtering when very low PAPR is required, which results in a relatively high computational complexity.[1]

D. Proposed MA Scheme and Contributions

In this work, we propose a MA scheme for extra-WBAN uplink, which does not need to apply the HS constraint to the FD signal. This could be seen as an extension of the scheme introduced in [39]. With this new scheme, called O-ROFDMA (R standing for real-valued), only the real part of the TD signal is transmitted. A similar approach was proposed in [40], where the complex-valued TD signal was used for phase rotation before removing the imaginary part to construct a continuous phase Flip-OFDM signal.[2] Focusing on the proposed O-ROFDMA, we show in this paper the advantage of the O-ROFDMA scheme compared with O-OFDMA and O-SCFDMA in terms of energy efficiency, PAPR, bit-error-rate (BER), and computational complexity. The particularity of the proposed study is that we take into account the limited DR of the LED and evaluate the performance of these schemes for both DCO and ACO signaling.

The main contributions of this work are:
- Proposing a HS-free O-ROFDMA signaling scheme for extra-WBAN uplink by transmitting only the real part of the TD signal;
- Performance comparison of the proposed scheme with O-OFDMA and O-SCFDMA considering realistic characteristics of opto-electronic components;

---

[1]Note that SCFDMA can be implemented as an add-on in the transmission chain, but it is likely to be less used in 5G, where it is considered as an optional mode only, besides the mandatory OFDMA.

[2]Flip-OFDM is an alternative approach to ACO-OFDM by which the negative parts of the O-OFDM signal are flipped before transmitting both positive and flipped parts in two consecutive sequences. Unlike Flip-OFDM, the continuous phase Flip-OFDM scheme does not require cyclic "midfix" between the positive and flipped sequences due to its phase continuity [40].
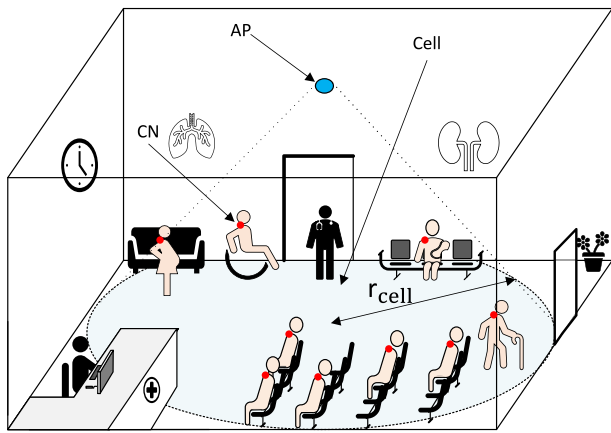
Fig. 1. Illustration of a health monitoring system in an emergency waiting room scenario by using IR extra-WBAN uplink for multiple patients, each one with a CN on the shoulder (the red bullet). A single AP is considered, placed on the ceiling.

- Demonstrating the suitability of the proposed O-ROFDMA scheme for the considered hospital scenario (i.e., emergency waiting room), as well as its relatively low computational complexity;
- Elucidating the MAI effect in O-ROFDMA due to the clipping noise;
- Studying the performance of O-ROFDMA by taking into account line-of-sight (LOS) link blockage due to random Tx orientations.

The remainder of the paper is organized as follows. In Section II, we present the system description in the context of the emergency waiting room scenario. Next, Section III presents the conventional O-OFDMA and O-SCFDMA schemes before describing in detail the proposed O-ROFDMA scheme in Section IV. Afterwards, Sections V and VI study the performance of O-ROFDMA and discuss its computational complexity, respectively. Lastly, Section VII concludes the paper.

Notation: $\ln(\cdot)$ stands for the natural logarithm, $E\{\cdot\}$ denotes the expected value and $.^*$ is the complex conjugate. Also, $\Re\{\cdot\}$ and $\Im\{\cdot\}$ stand for the real and imaginary parts, respectively.

II. SYSTEM DESCRIPTION

A. General Assumptions

An illustration of a typical emergency waiting room scenario in hospital with potentially up to sixteen patients inside is shown in Fig. 1. IR extra-WBAN links send medical information from the patients to an AP placed on the ceiling.

For the sake of simplicity and to focus on the performance of MA schemes, we consider only a single AP, i.e., a single-cell with radius of r_{cell}. For larger spaces, multiple APs can be used in a multi-cell [41], [42] or a single-cell [6] architecture. CNs are assumed to transmit the medical data at a rate of 500 Kbps for the extra-WBAN link, which satisfies the requirement of most health monitoring sensors, e.g., temperature, blood pressure, ECG, and SPO2 [43], [44].

CNs are considered to be placed on the shoulder of patients, which has been suggested as a rational choice in [10], [45], due to the relatively high possibility of having a LOS link to the AP as well as the patient comfort. At the Rx (i.e., AP) side, we consider the use of a simple PIN photodetector (PD) with no optical concentrator ensuring less sensitivity to background radiation (i.e., ambient noise), as compared to an avalanche PD, as well as a relatively large field-of-view (FOV).

At the Tx (i.e., CN) side, we consider the use of low-power IR LEDs (having a relatively wide beam), due to eye-safety issues given the relatively large number of patients in the emergency waiting room.[3] We consider a commercial IR LED as in [46], with a wavelength of 850 nm and maximum radiant intensity of 6.4 mW/sr. So, considering the simultaneous transfer of data from sixteen patients, the CNs equipped with such LEDs meet the IEC eye-safety requirement.

We assume that each CN is perfectly time synchronized with the AP. Note that, due to the limited mobility of patients in the room, the sensitivity to time synchronization errors (which is a recurrent problem in OFDMA-based systems [47]) is relatively low. Note that RF OFDMA requires multi-user time and frequency synchronization in order to avoid MAI and near-far problems, this is usually referred to as *initial ranging* [48]. However, the inherent absence of a carrier in O-OFDMA removes the need for frequency synchronization [49]. Also, a number of timing synchronization methods are reported in the literature [49], [50], [51], [52], which are mainly based on the transmission of training sequences, also used to acquire the channel state information (CSI).[4] We assume that the AP has a perfect knowledge of the CSI of all CNs.

B. Channel Model

For the sake of simulations simplicity, we neglect the non-LOS contribution in the received signal. In fact, this is a rational assumption given the relatively large dimensions of the emergency waiting room that we consider here. Considering a Lambertian radiation pattern for the LED at the Tx (i.e., the CN), and denoting the channel DC gain by H_{LOS}, we have [53]:

$$H_{\text{LOS}} = \begin{cases} \frac{A_{\text{PD}}(m+1)}{2\pi d^2}\cos^m(\varphi)\cos(\theta); & 0 \le \theta \le \theta_c \\ 0; & \theta > \theta_c, \end{cases} \quad (1)$$

where θ refers to the angle of the incident beam at the AP, A_{PD} is the PD's active area, θ_c denotes the FOV of the Rx (i.e., the AP), and d is the LOS link distance between the CN and the AP, as shown in Fig. 2. We have $d = \sqrt{D^2 + (h_{\text{AP}} - h_{\text{CN}})^2}$, where h_{CN} and h_{AP} stand for the heights of the CN and the AP, respectively. Also, D is the distance between the CN and the cell center, and φ refers to the Tx radiance angle that depends on the Tx orientation φ_{tx} (see Fig. 2). Moreover, m

---

[3]Note that, according to the IEC standard, the IR exposed to a cornea with an irradiance limit of 100 W/m^2 has no eye-hazard [11]. This irradiance limit can be calculated as the radiant intensity of 4 W/sr from a distance of 0.2 m, following the measurement condition in the standard.

[4]Training sequences from each CN can be sent to the AP in the uplink, based on which the estimated CSI at the AP is sent to the CNs via the downlink (which typically benefits from a higher signal-to-noise-ratio (SNR)).
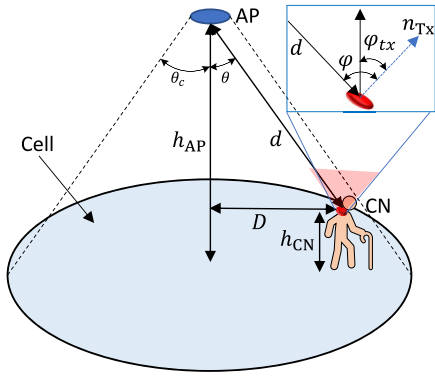
Fig. 2. Illustration of the LOS link between a CN and the AP. D is the distance between the patient (i.e., the CN) and the cell center and n_{Tx} refers to the normal vector corresponding to the CN.

Fig. 3. Block diagram of the DCO-OFDMA signaling scheme.

in (1) is the Lambertian order, related to the LED semi-angle at half power $\Phi_{1/2}$, $m = -\ln 2 / \ln(\cos \Phi_{1/2})$ [7].

Considering the transmit optical power $P_{t(\mathrm{opt})}$ and the PIN PD responsivity $\mathcal{R}$, the received photo-current is [7]:

$$i_{\mathfrak{r}} = \mathcal{R} H_{\mathrm{LOS}} P_{t(\mathrm{opt})}. \tag{2}$$

Denoting the load resistance of the Rx trans-impedance amplifier (TIA) by R_L, the received electrical power $P_{\mathfrak{r}}$ is:

$$P_{\mathfrak{r}} = i_{\mathfrak{r}}^2 R_L. \tag{3}$$

Considering a PIN PD at the AP, background and thermal noises are the dominant noise sources, modeled as zero-mean additive white Gaussian with the one sided power spectral density N_0 [7], [54]:

$$N_0 \approx 4 K_B T / R_L + 2 q_e I_a, \tag{4}$$

where, K_B is the Boltzmann's constant, T refers to the temperature, q_e stands for the electron charge, and I_a denotes the ambient current noise.

III. CONVENTIONAL MA SCHEMES

Here, we present a brief description of the "conventional" MA schemes, i.e., O-OFDMA and O-SCFDMA, for the two cases of DCO and ACO signaling.

A. DCO-OFDMA

Figure 3 shows the block diagram of DCO-OFDMA signaling. First, the collected data bits from sensors are grouped together by the serial to parallel (S/P) converter and mapped into M-QAM complex symbols $\check{X}_{\acute{k}}$, $\acute{k} = 0, 1 \ldots, \mathcal{M} - 1$. Here, $\mathcal{M}$ refers to the number of data-carrying symbols (i.e., subcarriers) per user.[5] Then, these $\mathcal{M}$ symbols are mapped into a subset of subcarriers X_k, $k = 0, 1 \ldots, N - 1$, where N is the total number of subcarriers before the HS block. Considering a maximum $\mathcal{L}$ number of patients, the total number of subcarriers is $N = \mathcal{ML}$. We will explain in detail the considered subcarrier mapping technique in Section V. To obtain a real

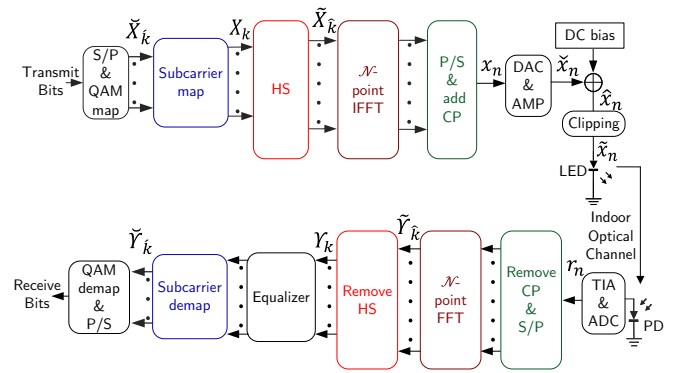[5]In the sequel, we use the two terms of "subcarriers" and "symbols" interchangeably.

TD OFDMA signal, HS constraint is then imposed on X_k to get $\tilde{X}_{\hat{k}}$, $\hat{k} = 0, 1 \ldots, \mathcal{N} - 1$; $\mathcal{N} = 2N + 2$, such that,

$$\tilde{X}_{\hat{k}} = [0, X_0, X_1, \ldots, X_{N-1}, 0, X_{N-1}^* \ldots, X_0^*].$$

Then, an $\mathcal{N}$-point inverse-fast-Fourier transform (IFFT) is performed, that generates the real-valued TD signal x_n:

$$x_n = \frac{1}{\sqrt{\mathcal{N}}} \sum_{\hat{k}=0}^{\mathcal{N}-1} \tilde{X}_{\hat{k}} \exp\left(j \frac{2\pi n \hat{k}}{\mathcal{N}}\right) ; \ n = 0, 1, \ldots, \mathcal{N} - 1. \tag{5}$$

After parallel to serial conversion (P/S) and adding a cyclic prefix (CP) of length $\mathcal{N}_{\mathrm{CP}}$ at the end of each frame, the resulting signal is passed through a digital to analog converter (DAC) and an amplifier (AMP) before the addition of a DC bias $\mathcal{B}_{\mathrm{DC}}$ to obtain $\hat{x}_n$:

$$\hat{x}_n = \check{x}_n + \mathcal{B}_{\mathrm{DC}}, \tag{6}$$

where $\check{x}_n$ denotes the amplified signal (see Fig. 3). To fix $\mathcal{B}_{\mathrm{DC}}$, the DR of the LED should be taken into account, as explained later in Section IV-C. Lastly, after lower and upper clipping $\hat{x}_n$, the resulting signal $\tilde{x}_n$ will drive the LED.

At the Rx, after photo-detection and removing the DC, the obtained electrical signal is amplified by a TIA and passed to an analog to digital converter (ADC) to generate a discrete-time signal r_n. Then, after removing the CP and S/P conversion, $\mathcal{N}$-point fast-Fourier-transform (FFT) is done on the signal, resulting in:

$$\tilde{\Upsilon}_{\hat{k}} = \frac{1}{\sqrt{\mathcal{N}}} \sum_{n=0}^{\mathcal{N}-1} r_n \exp\left(-j \frac{2\pi n \hat{k}}{\mathcal{N}}\right) ; \ \hat{k} = 0, 1, \ldots, \mathcal{N} - 1. \tag{7}$$

Afterwards, after removing HS from $\tilde{\Upsilon}_{\hat{k}}$, single-tap equalization is performed on the resulting signal Υ_k. Then, the signal is passed through a subcarrier demapping block to obtain symbols $\check{\Upsilon}_{\acute{k}}$ corresponding to the desired user data before P/S conversion and QAM demodulation.

B. ACO-OFDMA

In ACO-OFDMA, only odd subcarriers are used for signal transmission. After applying the HS constraint, the input
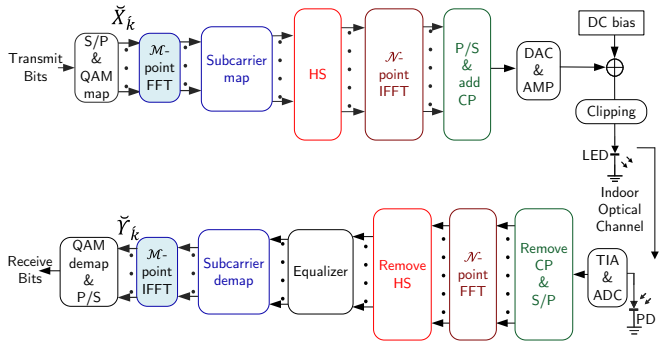
Fig. 4. Block diagram of the DCO-SCFDMA signaling scheme. The blue-shaded blocks highlight the additional $\mathcal{M}$-point FFT/IFFT, compared to DCO-OFDMA in Fig. 3.

symbol frame $\tilde{X}_{\hat{k}}$ before the IFFT has the following structure,

$$\tilde{X}_{\hat{k}} = \begin{bmatrix} 0, X_0, 0, X_1, \ldots, 0, X_{N-1}, 0, X^*_{N-1}, \ldots, 0, X^*_0 \end{bmatrix}.$$

After the IFFT, the negative samples can be clipped without loss of information due to the anti-symmetry property of x_n [55]. The subsequent steps for ACO-OFDMA are similar to those of DCO-OFDMA, described in the previous subsection. Note that ACO-OFDMA also requires a DC bias to be added to $\check{x}_n$ to adapt to the actual LED I-V characteristics [24], as will be explained in Section IV-C.

C. DCO-SCFDMA

The block diagram of the DCO-SCFDMA scheme is shown in Fig. 4. QAM mapped symbols from each user are precoded by an $\mathcal{M}$-point FFT before subcarrier mapping and applying HS, and $\mathcal{N}-$point IFFT. This allows to reduce the signal PAPR at the cost of increased complexity. The other steps of signal transmission are similar to the case of DCO-OFDMA, explained above. At the Rx side, after $\mathcal{N}-$point FFT, equalization, and subcarrier demapping, an $\mathcal{M}-$point IFFT is applied to the resulting signal.

D. ACO-SCFDMA

Similar to the case of O-OFDMA, described in Section III-B, by ACO-SCFDMA, the transmit signal frame follows the same steps as for DCO-SCFDMA except that only the odd subcarriers are used for data transmission.

IV. DESCRIPTION OF THE PROPOSED MA SCHEME

As mentioned previously, in our proposed ROFDMA scheme, only the real part of the TD signal is transmitted, hence removing the need for HS. Lets first explain the theoretical foundation of recovering a FD signal from the real part of its IFFT. Consider the FD symbols X_k after subcarrier mapping without imposing HS, and the corresponding TD signal $x_{n'}$, $n' = 0, 1 \ldots, N - 1$. We have [56]:

$$\begin{cases} \frac{1}{2}\begin{bmatrix} X_k + X^*_{N-k} \end{bmatrix} \xrightarrow{\text{IFFT}} \Re\{x_{n'}\} \\ \frac{1}{2}\begin{bmatrix} X_k - X^*_{N-k} \end{bmatrix} \xrightarrow{\text{IFFT}} j\Im\{x_{n'}\} \end{cases} \tag{8}$$

(a) Real-valued FD signal   (b) Complex conjugate & reversed
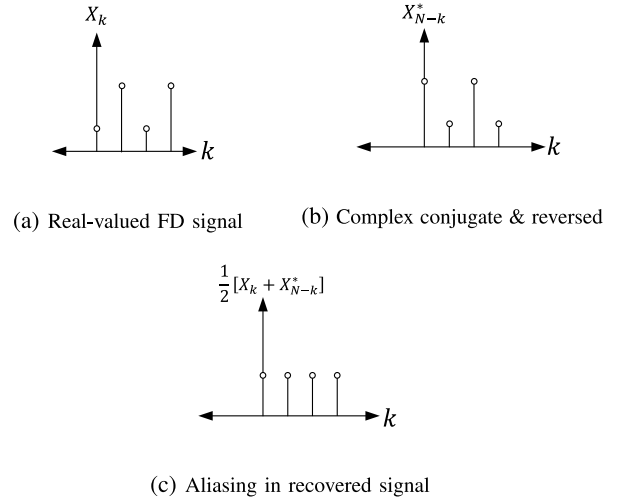
(c) Aliasing in recovered signal

Fig. 5. Illustrating FD aliasing in a recovered signal from the real part of its IFFT output: (a) Real-valued subcarriers in a FD signal, with the total number of subcarriers $N = 4$, (b) The complex conjugate and reversed version of the FD signal, (c) The FFT output signal taking into account only the real part, showing FD aliasing.

(a) The original FD signal   (b) Zero padded FD signal

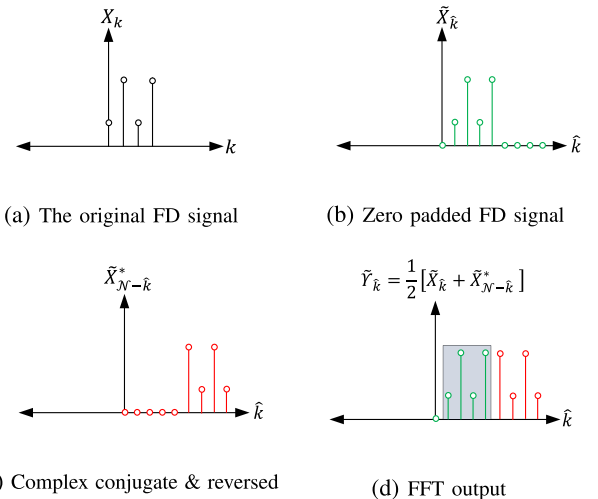(c) Complex conjugate & reversed   (d) FFT output

Fig. 6. Illustration of recovering a FD signal from the real part of its zero-padded IFFT output: (a) Real-valued subcarriers in a FD signal with $N = 4$, (b) Zero-padded FD signal with length $2N + 1$, (c) Complex conjugate subcarriers of the zero-padded FD signal mapped in reverse-order, (d) FFT output of the signal taking into account only the real part, showing no FD aliasing. The shaded region shows the recovered signal X_k.

Here, X^*_{N-k} refers to the complex conjugate and time-reversed version of X_k. Given (8), it is obvious that recovering X_k from the real part of $x_{n'}$ alone is not possible. This is due to the complex-conjugate term X^*_{N-k} that overlaps with the subcarriers X_k and causes FD aliasing, as illustrated in Fig. 5.

The effect of aliasing can be avoided by padding a zero at the begining of the symbol frame X_k and an adequate number of zeros (at least N) at the end [57].[6] This increases the number of subcarriers for IFFT to $\mathcal{N} \geq 2N + 1$. Based on this, Fig. 6 illustrates the reconstruction of the FD signal from the real

[6]Note that, it is essential to pad a zero at the beginning of the frame if the signal is complex-valued [57].
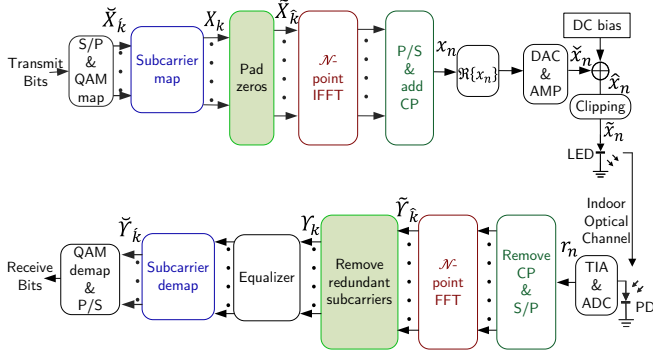
Fig. 7. Block diagram of the DCO-ROFDMA signaling scheme. The green-shaded blocks highlight the zero-padded mapped sub-carriers (instead of imposing HS) at the Tx, and removal of redundant sub-carriers at the Rx, compared to DCO-OFDMA in Fig. 3.

Fig. 8. I-V characteristics of the LED, HDN1102W-TR [46].

part of the TD signal. Given the real-valued FD symbols X_k in Fig. 6(a), the symbols $\tilde{X}_{\hat{k}}$ of the extended frame (with zero padding, in Fig. 6(b)) are given by:

$$\tilde{X}_{\hat{k}} = \begin{cases} 0; & \hat{k} = 0, \\ X_{\hat{k}-1}; & \hat{k} = 1, 2 \dots, N, \\ 0; & \hat{k} = N+1, \dots, \mathcal{N}-1. \end{cases} \quad (9)$$

Because of zero padding, there will be no FD aliasing between the complex conjugate and time-reversed version of the signal $\tilde{X}_{\hat{k}}$ (see Fig. 6(c)), allowing the correct recovery of the original signal X_k, as seen in Fig. 6(d).

A. DCO-ROFDMA

Figure 7 shows the block diagram of DCO-ROFDMA signaling. The mapped subcarriers X_k in the FD signal are zero-padded (before the IFFT block) instead of imposing HS[7] as in (9). Then, only the real part of the TD signal $\Re\{x_n\}$ is used for transmission, following the same steps described for DCO-OFDMA.

At the Rx side, the signal processing steps are similar to DCO-OFDMA up to the FFT block. The FD signal $\tilde{\Upsilon}_{\hat{k}}$ is recovered by performing FFT only on $\Re\{x_n\}$:

$$\tilde{\Upsilon}_{\hat{k}} = \begin{cases} X_{\hat{k}-1}; & \hat{k} = 1, 2, \dots, N, \\ X^*_{\mathcal{N}-1-\hat{k}}; & \hat{k} = N+1, \dots, \mathcal{N}-1, \\ 0; & \text{elsewhere}. \end{cases} \quad (10)$$

After the FFT block, the transmitted symbols are recovered:

$$\Upsilon_k = \tilde{\Upsilon}_k; \quad k = 1, 2, \dots, N. \quad (11)$$

Then, channel equalization, subcarrier- and QAM-demapping are performed in order to recover the transmitted bits.

B. ACO-ROFDMA

In ACO-ROFDMA, after zero padding, the transmit symbols $\tilde{X}_{\hat{k}}$ before the IFFT block have the same frame structure as

for DCO-OFDMA except that only even subcarriers are used to transmit data:

$$\tilde{X}_{\hat{k}} = \left[0, 0, X_0, 0, X_1, 0, \dots, X_{N-1}, 0, \underbrace{0, \dots, 0}_{(2N+2) \text{ times}} \right].$$

The rest of the processing steps are the same as for DCO-ROFDMA. Note that, in contrast to the scheme presented in [39], it is essential to transmit information in the even subcarriers to ensure orthogonal cardinal sine (sinc) shape.

C. Setting DC Bias and Clipping

In practice, a DC bias is added to the TD signal in order to adapt the signal to the LED DR [24]. We consider the commercial LED model HDN1102W-TR, with I-V characteristics shown in Fig. 8 [46].

Note that the LED operates almost linearly within the voltage range of 1.38 to 1.62 V. For the sake of simplicity, we consider the approximate linearized characteristics in our analysis, (the red plot in the figure).[8] Considering these lower and upper clipping levels, we set $\mathcal{B}_{\text{DC}} = 1.38$ V for ACO schemes. For DCO schemes, we set $\mathcal{B}_{\text{DC}}$ to the mid point between the upper and lower clipping bounds, i.e., 1.5 V, to affect the TD signal equally.

V. PERFORMANCE ANALYSIS

A. Parameter Specification and Performance Metrics

We present here a set of numerical results to study the performance of the proposed O-ROFDMA scheme for extra-WBANs in the emergency waiting room scenario. We consider the number of patients $\mathcal{L} = 16$ and bit rate $R_b = 500$ Kbps per user. Also, $\mathcal{M} = 4$ subcarriers per user are considered with the total number of subcarriers $N = 64$. The other simulation parameters are summarized in Table I, where the LED parameters correspond to the I-V characteristics in Fig. 8.

---

[7]Note that, in order to keep the same spectral efficiency as for the conventional MA schemes which employs HS, we add one extra zero at the end of the frame $\tilde{X}_{\hat{k}}$ such that $\mathcal{N} = 2N + 2$.
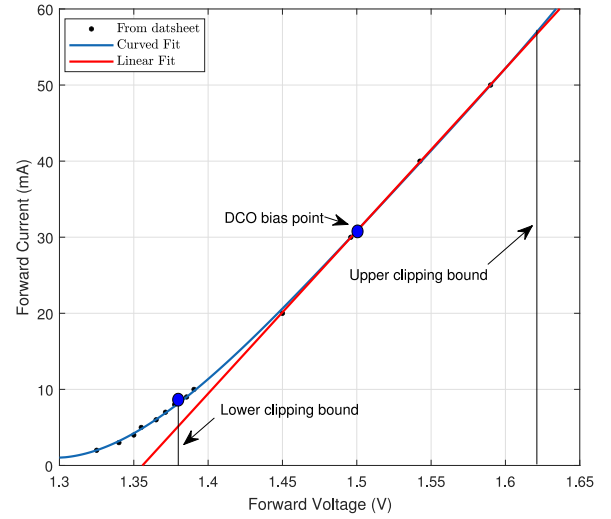
[8]Note that a digital predistorter can be employed at the Tx to reduce the effect of LED non-linearity [58].

TABLE I
PARAMETERS USED FOR NUMERICAL SIMULATIONS

| Parameter	Symbol	Value
Max. number of users	$\mathcal{L}$	16
Data-rate per user	R_b	500 Kbps
Cell radius	r_{cell}	3 m
CN height	h_{CN}	1 m
AP height	h_{AP}	3 m
LED wavelength [46]	λ	850 nm
LED semi-angle at half power	$\Phi_{1/2}$	60°
LED BW [46]	—	20 MHz
Power conversion efficiency [46]	α	0.8
Tx orientation angle intervals	φ_{tx}	-60°−60°
PD responsivity	$\mathcal{R}$	0.6 A/W
PD active area	A_d	1 cm²
Rx FOV	θ_c	70°
TIA resistor value	R	50 Ω
Rx noise temperature	T	300 K
No. of mapped subcarriers	N	64
Subcarriers allocated per user	$\mathcal{M}$	4
CP length	$\mathcal{N}_{\text{CP}}$	2
DAC/ADC	—	8 bits
DC-bias, DCO	$\mathcal{B}_{\text{DC(DCO)}}$	1.50 V
DC-bias, ACO	$\mathcal{B}_{\text{DC(ACO)}}$	1.38 V
Upper clipping	—	1.62 V
Lower clipping	—	1.38 V
Target BER	BER_{th}	10^{-3}
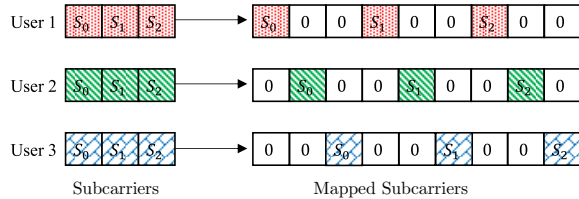
Fig. 9. An example of interleaved subcarrier mapping for the case of $\mathcal{L} = 3$ users, each having three symbols denoted by S_0, S_1 and S_2.

Note that we consider 8-bit ADC and DAC and the presented numerical results take into account the corresponding quantization noise. Also, unless otherwise specified, for the sake of simulation simplicity, the CNs are considered to point straight upward (towards the ceiling), i.e., $\varphi_{tx} = 0$ in Fig. 2. Interleaved subcarrier mapping is applied to each user symbols, as illustrated in Fig. 9 for the case of three users. This leads to a lower PAPR for the case of SCFDMA [59], in addition to mitigating burst errors. The signal PAPR is considered as the ratio between the peak electrical power of the TD signal (before clipping) to its average power, defined as $E\{x_n^2\}$. The PAPR performance is typically studied by considering its complementary cumulative distribution function (CCDF) [60].

The link performance is evaluated in terms of the average BER as a function of the electrical transmit power $P_{t(\text{elec})} =$
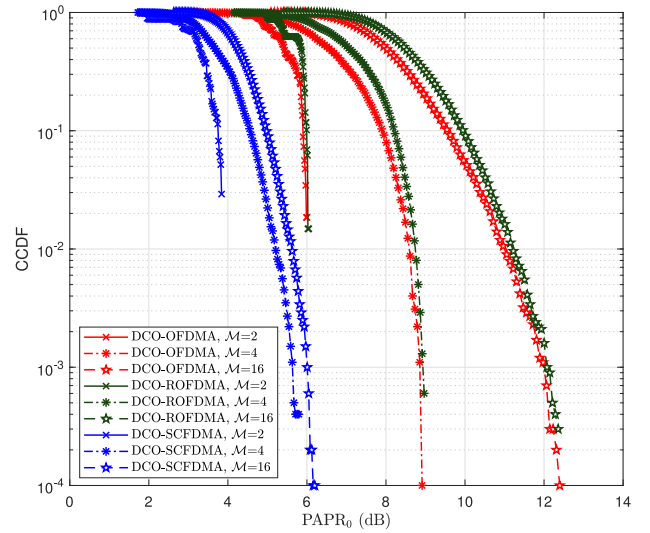

Fig. 10. CCDF plots of PAPR for DCO-OFDMA, DCO-SCFDMA and DCO-ROFDMA schemes, considering different numbers of data-carrying symbols $\mathcal{M}$ per user and the 16-QAM constellation.

$E\{\tilde{x}_n^2\}$ or the electrical SNR[9] per bit, $E_{b(\text{elec})}/N_0$, where $E_{b(\text{elec})} = P_{t(\text{elec})}/R_b$. Note, $P_{t(\text{elec})} = P_{t(\text{opt})}/\alpha$ with α being the electrical-to-optical power conversion efficiency of the LED. Given the considered LED I-V characteristic curve in Fig. 8, the part of $P_{t(\text{elec})}$ corresponding to the DC bias equals 7 mW and 46.2 mW for ACO and DCO schemes, respectively.

For random link scenarios (e.g., the case of randomly-oriented Txs, presented later), the outage probability is considered, which is defined as the probability that the BER exceeds a given threshold, BER_{th}.

Due to the limited modulation BW of the LED, an important parameter is the required BW per user, which depends on the signaling scheme. Considering M-QAM constellation, the spectral efficiencies of DCO and ACO schemes are [23]:

$$\Gamma_{\text{DCO}} = \frac{\log_2(M)N}{\mathcal{N} + \mathcal{N}_{\text{CP}}}, \quad \Gamma_{\text{ACO}} = \frac{\log_2(M)N}{2\mathcal{N} + \mathcal{N}_{\text{CP}}} \quad (\text{bps/Hz}). \tag{12}$$

Remember that $\mathcal{N} = 2N + 2$ with N the number of mapped subcarriers. As ACO schemes use only half of the subcarriers, the corresponding spectral efficiency will be half of the corresponding DCO scheme, keeping the same constellation size and number of subcarriers. To make a fair comparison between DCO and ACO-based schemes, we fix the spectral efficiency by setting M accordingly. The spectral efficiencies per user are then given by $\Gamma_{\text{DCO}}/\mathcal{L}$ and $\Gamma_{\text{ACO}}/\mathcal{L}$, with the corresponding required BWs per user as:

$$B_{\text{DCO}} = \frac{R_b}{\Gamma_{\text{DCO}}/\mathcal{L}} = \frac{R_b \mathcal{L}}{\Gamma_{\text{DCO}}}, \quad B_{\text{ACO}} = \frac{R_b \mathcal{L}}{\Gamma_{\text{ACO}}}. \tag{13}$$

B. PAPR Analysis

Figure 10 compares the PAPR of the proposed O-ROFDMA scheme with O-OFDMA and O-SCFDMA for the case of DCO

---

[9]Note that the SNR is defined here at the input of the Rx. For instance, for the case of ACO-OFDM signaling, the SNR refers to the noise at the Rx input before applying the FFT. In other words, our SNR definition takes into account the noise on both odd and even subcarriers [61].
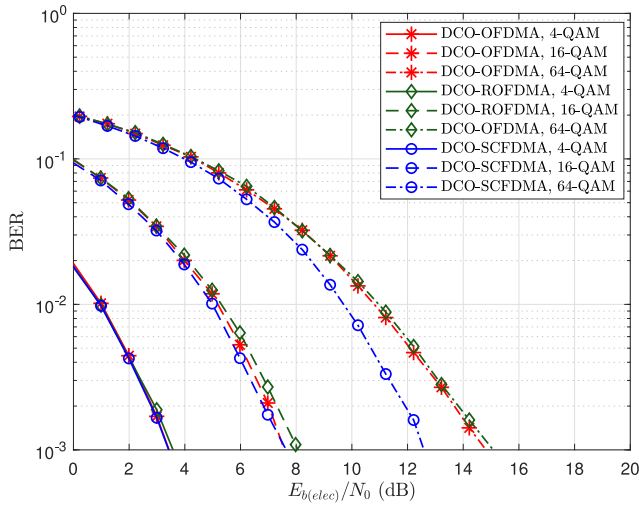
Fig. 11. Contrasting BER performances of DCO schemes, for spectral efficiencies of $\approx$ 1 bps/Hz (4-QAM), $\approx$ 2 bps/Hz (16-QAM), and $\approx$ 3 bps/Hz (64-QAM). $P_{t(\text{elec})} = 48$ mW. All users placed at $D = 3$ m from the AP.

Fig. 12. Contrasting BER performances of ACO schemes for spectral efficiencies of $\approx$ 0.5 bps/Hz (4-QAM), $\approx$ 1 bps/Hz (16-QAM), and $\approx$ 1.5 bps/Hz (64-QAM). $P_{t(\text{elec})} = 23$ mW. All users placed at $D = 3$ m from the AP.

signaling with 16-QAM modulation and different numbers $\mathcal{M}$ of data carrying symbols. We notice that the PAPR performances of DCO-ROFDMA and DCO-OFDMA are almost the same, while being largely outperformed by DCO-SCFDMA, as expected. This is due to the additional DFT precoder used in SCFDMA (see blue-shaded blocks in Fig. 4), which spreads the energy of each symbol across all subcarriers prior to the $\mathcal{N}$-point IFFT [37], [38], [62].

Also, as expected, PAPR increases with increased $\mathcal{M}$. Given the typically small number of symbols $\mathcal{M}$ for low data-rate medical applications, we can conclude that the signal PAPR remains relatively low. Note that for low CCDF values, the PAPR is almost the same regardless of the constellation size, in particular, for small $\mathcal{M}$ (results not shown).

C. BER Performance

To study the BER performance, we consider the most limiting case of maximum channel attenuation, i.e., when all users are placed at the cell edge, corresponding to $D = 3$ m from the center of the cell.

1) DCO Signaling: In this case, given $\mathcal{L} = 16$ and $\mathcal{M} = 4$, $\mathcal{N} = 130$ after imposing the HS. Then, considering $R_b = 500$ Kbps, Fig. 11 shows the BER performance versus $E_{b(\text{elec})}/N_0$ for 4-QAM, 16-QAM and 64-QAM constellations, corresponding to the spectral efficiencies $\Gamma_{\text{DCO}} \approx 1, 2$, and 3 bps/Hz, and the required transmission BWs $B_{\text{DCO}} = 8, 4$, and 2.67 MHz, respectively. We have fixed $P_{t(\text{elec})}$ to 48 mW, which ensures a low BER for DCO schemes, as we will later show in Section V-D. We notice that the BER performances of DCO-OFDMA and DCO-ROFDMA are almost the same, while being outperformed by DCO-SCFDMA, in particular, for 64-QAM. This is due to the relatively low PAPR of SCFDMA, resulting in lower clipping noise.

2) ACO Signaling: In this case, considering the same R_b and QAM constellation sizes as above, the required transmission BWs are $B_{\text{ACO}} = 16, 8$, and 5.33 MHz, corresponding to the spectral efficiencies $\Gamma_{\text{ACO}} \approx 0.5, 1$, and 1.5 bps/Hz,
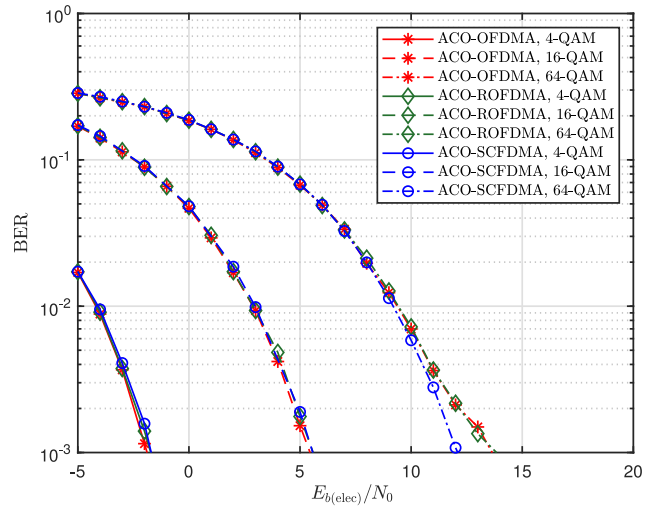
respectively. Note that B_{ACO} values are still below the considered LED BW of 20 MHz. Here, $\mathcal{N} = 258$ and $P_{t(\text{elec})}$ is set to 23 mW, which is lower than that for DCO schemes due to the smaller required bias $\mathcal{B}_{\text{DC}}$, as explained in Section V-D. Note that a BER comparison between ACO and DCO schemes does not make sense here, given the different $P_{t(\text{elec})}$ considered. Figure 12 shows the corresponding BER performances where we notice nearly the same performance for ACO-OFDMA and ACO-ROFDMA, while ACO-SCFDMA outperforms both for 64-QAM, as expected. For reduced $\Gamma_{\text{ACO}} \approx 0.5$ bps/Hz, lower SNRs are reasonably required to attain a target BER.

D. Electrical Power Efficiency

Let us define the electrical power efficiency as the required $P_{t(\text{elec})}$ to achieve a target BER. We consider the same scenario as in the previous subsection, where the users are placed at the same position at the distance $D = 3$ m. BER plots of the different considered schemes are compared in Fig. 13 for the spectral efficiency of $\approx$ 1 bps/Hz, where 16-QAM and 4-QAM constellations are considered for ACO and DCO schemes, respectively. Here, $P_{t(\text{elec})}$ is changed by varying the amplitude of x_n (see Fig. 3) taking into account $\mathcal{B}_{\text{DC}}$. To focus on the effect of signal clipping, we set relatively high $E_{b(\text{elec})}/N_0 = 15$ dB, which should potentially result in a low BER, as seen in Fig. 12.

One can notice the BER degradation at relatively large $P_{t(\text{elec})}$ due to the clipping noise.[10] Also, the ACO schemes require approximately 35 mW less $P_{t(\text{elec})}$ to obtain a target BER, compared to DCO schemes. The performance of SCFDMA is close to those of OFDMA and ROFDMA for

---

[10]To go more into detail, the BER leveling effect around 0.3 that we observe at relatively high transmit powers for ACO schemes is due to signal clipping of "outer points" in the 16-QAM constellation. When $P_{t(\text{elec})}$ is increased too much (not shown in the figure), the BER jumps to 0.5 as all 16-QAM constellations points get clipped. Also, note that increasing too much the amplitude of x_n does not necessarily result in an increase in $P_{t(\text{elec})}$, as this latter relies on the symbols after clipping.
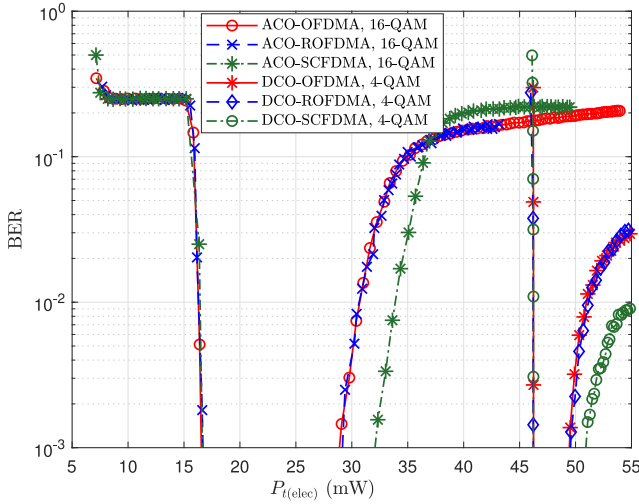
Fig. 13. BER versus $P_{t(\mathrm{elec})}$ performance comparison between ACO and DCO schemes for fixed $E_{b(\mathrm{elec})}/N_0 = 15$ dB and the spectral efficiency of ≈ 1 bps/Hz using 16-QAM and 4-QAM with $\mathcal{M} = 4$ for ACO and DCO schemes, respectively. All users placed at $D = 3$ m from the AP.
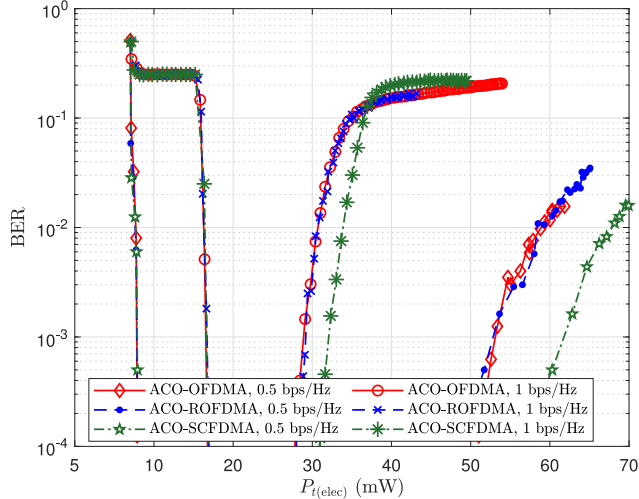

Fig. 14. BER performance comparison of ACO schemes for the spectral efficiency of ≈ 0.5 bps/Hz (4-QAM, $\mathcal{M} = 4$) and ≈ 1 bps/Hz (16-QAM, $\mathcal{M} = 4$) with respect to different average electrical transmit power $P_{t(\mathrm{elec})}$, for a fixed $E_{b(\mathrm{elec})}/N_0 = 15$ dB. Users are placed at $D = 3$ m from the AP.

both DCO and ACO signaling. Meanwhile, as expected, due to the low PAPR, SCFDMA is less impacted by clipping noise for relatively large $P_{t(\mathrm{elec})}$.

Remember from Section IV-C that, due to the added DC bias, the minimum required $P_{t(\mathrm{elec})}$ for ACO and DCO schemes is 7 and 46.2 mW, respectively. The slope of the BER at relatively low $P_{t(\mathrm{elec})}$ that is noticed for ACO schemes is due to the effect of the quantization noise due to the ADC at very low *effective* signal powers (i.e., excluding the part of the power related to $\mathcal{B}_{\mathrm{DC}}$). This effect is rather negligible for a small constellation size, i.e., the case of DCO-schemes with 4-QAM. At the aforementioned $P_{t(\mathrm{elec})}$ where the *effective* signal power equals zero, BER = 0.5.

Let us now compare the performance of ACO schemes for spectral efficiencies of ≈ 0.5 and ≈ 1 bps/Hz, as shown in Fig. 14. As expected, a lower $P_{t(\mathrm{elec})}$ is required to attain a
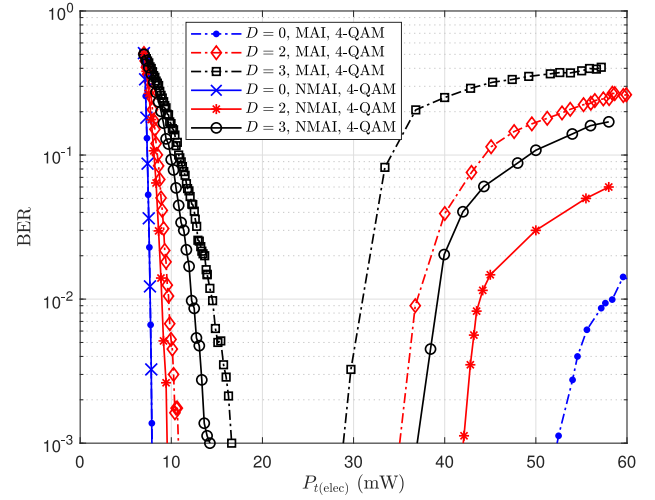
(a) $\Gamma_{\mathrm{ACO}} \approx 0.5$ bps/Hz, (4-QAM, $\mathcal{M} = 4$)
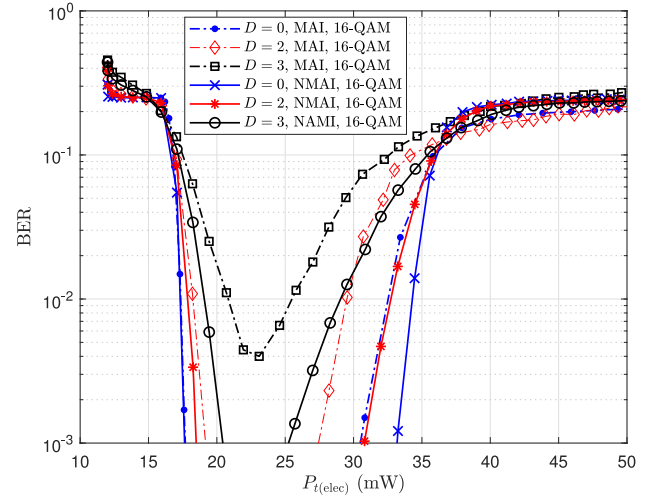
(b) $\Gamma_{\mathrm{ACO}} \approx 1$ bps/Hz (16-QAM, $\mathcal{M} = 4$)

Fig. 15. BER versus the average electrical transmit power for different distances D of the desired user from the AP; (a) $\Gamma_{\mathrm{ACO}} \approx 0.5$ bps/Hz, (4-QAM, $\mathcal{M} = 4$); (b) $\Gamma_{\mathrm{ACO}} \approx 1$ bps/Hz (16-QAM, $\mathcal{M} = 4$). For MAI case, the other 15 users are positioned at the cell center. N_0 is set to 3.93×10^{-22} W/Hz according to (4) and the parameters specified in Table I.

target BER for a lower spectral efficiency, which is due to using a smaller constellation size at the cost of increased signal BW. Moreover, for 4-QAM case ($\Gamma_{\mathrm{ACO}} \approx 0.5$ bps/Hz), clipping noise affects the link performance for relatively large transmit powers, i.e., $P_{t(\mathrm{elec})} \gtrsim 50$ mW, while ACO-SCFDMA again shows a superior performance due to a lower PAPR.

E. MAI Effect

To elucidate the effect of MAI, lets focus on ACO-ROFDMA as an appropriate transmission scheme due to its lower transmit power requirement (as shown in the results of Fig. 13). Figures 15(a) and 15(b) show the BER performances of a desired user with different distances D from the cell center for $\Gamma_{\mathrm{ACO}} \approx 0.5$ and 1 bps/Hz, respectively. The other 15 users are placed at the cell center (hence, potentially causing

(a) Before upper clipping
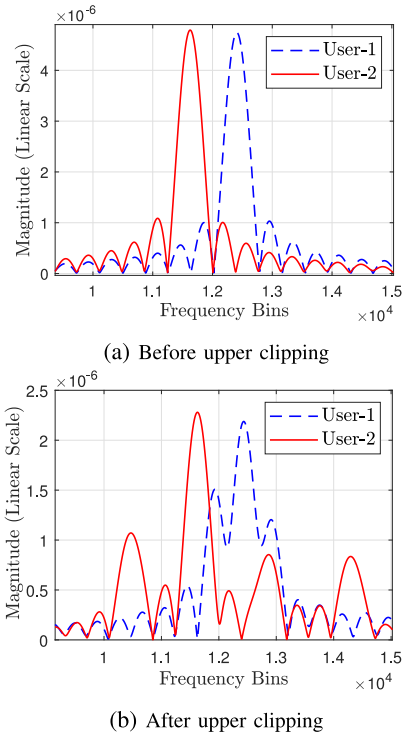

(b) After upper clipping

Fig. 16. Spectral magnitude of ACO-ROFDMA signals for the case of two users: (a) Without signal clipping, (b) With the effect of clipping noise.

the maximum MAI), and the same $P_{t(\text{elec})}$ is set to all users. We have also presented as benchmark the BER plots for the case where there is only the desired user in the cell, indicated by NMAI (standing for No-MAI). Obviously, the BER degrades by increasing D due to the decrease in the Rx SNR. The important observation is the difference between MAI and NMAI cases as one would expect no performance degradation when considering multiple users. This is, in fact, due to signal clipping, which affects the orthogonality between users' signals. The degradation is more noticeable for increased D due to the well-known near-far problem.

To clarify this, consider the case of two users with 4-QAM modulation with rectangular pulse shaping on the TD signal at the Tx. After applying ACO-ROFDMA, the spectra of the two users' signals should normally be in the form of two orthogonal sincs, as illustrated in Fig. 16(a). However, when signal clipping is applied at the Tx, this orthogonality is lost due to the *spectral regrowth* in the adjacent subcarriers, see Fig. 16(b). As a result, signal reception is effectively affected by MAI, which is more pronounced at relatively high transmit powers, for larger constellation sizes, and with increasing D, as can be seen from Fig. 15.

For the sake of completeness, consider now the more realistic case of random Tx orientations. (So far, we have considered that all Txs are pointing toward the ceiling in order to avoid costly simulations and to focus on the performance study of the MA schemes.) For this, the φ_{tx} of the CNs in Fig. 2 are generated randomly according to a zero-mean Gaussian distribution, while being limited to the interval $(-60°, 60°)$. Nevertheless, still only the LOS contribution is taken into account, which is justified by the considered large room dimensions, and hence,
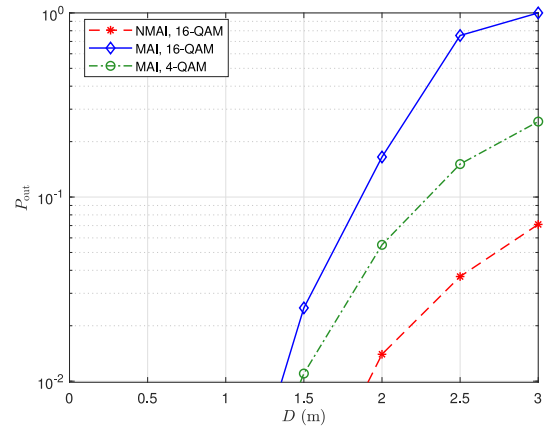

Fig. 17. P_{out} performance of ACO-ROFDMA due to random Tx orientation for different D of the desired user and $\Gamma_{\text{ACO}} \approx 0.5$ bps/Hz (4-QAM, $\mathcal{M} = 4$), and ≈ 1 bps/Hz (16-QAM, $\mathcal{M} = 4$).

the rather negligible contribution of non-LOS links. Based on 10^5 random orientations for all users, P_{out} results as a function of D are shown in Fig. 17 for the cases of MAI and NMAI, considering $\text{BER}_{\text{th}} = 10^{-3}$. $P_{t(\text{elec})}$ is set to 23 mW, corresponding to a low BER, based on the results of Fig. 15. For the case of 4-QAM with NMAI, P_{out} is less than 10^{-3} and the corresponding plot is not shown. As expected, P_{out} increases as the user moves from the center of the cell to the edge due to the higher probability of losing the LOS link. Given that the required P_{out} for WBAN application is about 10^{-2} [6], this is achieved for $D \lesssim 1.5$ m and $D \lesssim 1.4$ m for 4-QAM and 16-QAM cases, respectively.

In practice, given the large dimensions of an emergency waiting room, in order to increase the link robustness, multiple APs should be employed [6] with short enough distance between them, e.g., less than 3 m for the case of 16-QAM.

VI. COMPLEXITY ANALYSIS

To evaluate the computational complexity of the considered signaling schemes, we focus on the complexity of realizing the $\mathcal{N}$-point IFFT/FFT for a number $\mathcal{N}$ of mapped subcarriers, as well as the extra $\mathcal{M}$-point FFT/IFFT used in O-SCFDMA.

The computational complexity of IFFT/FFT is related to the floating-point operations (FLOPs) for real additions and multiplications [63]. Without loss of generality, we consider a radix-2-based algorithm, for the sake of simplicity, using which an $\mathcal{N}$-point FFT/IFFT requires approximately $5\mathcal{N} \log_2(\mathcal{N})$ arithmetic operations [64]. For O-ROFDMA, the FLOP count at the Tx is reduced by a factor of 2 due to applying padded zeros in the last $\mathcal{N}$ subcarriers. Figure 18 illustrates an example of radix-2 IFFT algorithm for DCO-ROFDMA considering $\mathcal{N} = 8$. At Stage-1, given a zero in one of the symbols in a butterfly of length 2, no arithmetic operation is required, and the outputs follow the input symbols. Therefore, the first half of symbols are in fact identical copies of the second-half symbols, see Stage-2. This way, no arithmetic operation is required for half of the symbols (shown in red color), thus reducing the computational complexity by a factor of 2.
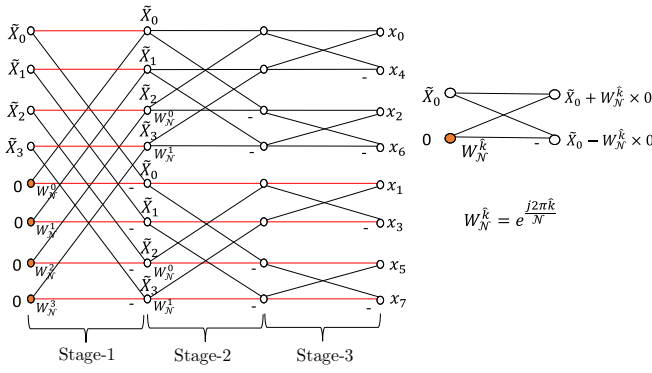
Fig. 18.   Illustration of a radix-2 IFFT algorithm for a length $\mathcal{N} = 8$, considering DCO-ROFDMA. $W_{\mathcal{N}}^{\hat{k}}$ is the so-called *twiddle factor* [56].

TABLE II
COMPUTATIONAL COMPLEXITY OF DIFFERENT MA SCHEMES

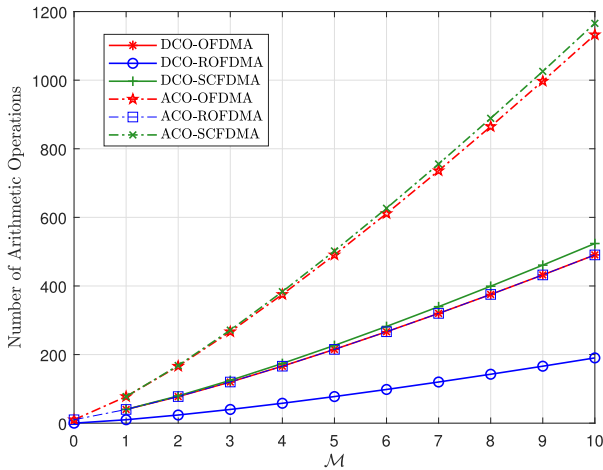| MA Scheme	Tx	Rx
DCO-OFDMA	$5\mathcal{N}\log_2(\mathcal{N})$	$5\mathcal{N}\log_2(\mathcal{N})$
DCO-SCFDMA	$5\mathcal{M}\log_2(\mathcal{M}) + 5\mathcal{N}\log_2(\mathcal{N})$	$5\mathcal{N}\log_2(\mathcal{N}) + 5\mathcal{M}\log_2(\mathcal{M})$
DCO-ROFDMA	$5\frac{\mathcal{N}}{2}\log_2(\frac{\mathcal{N}}{2})$	$5\mathcal{N}\log_2(\mathcal{N})$

Fig. 19.   Complexity analysis of different schemes in terms of required number of arithmetic operations at the Tx versus the number of data-carrying symbols $\mathcal{M}$; $\mathcal{N} = \mathcal{M}\mathcal{L}$ with $\mathcal{L} = 16$.

The computational complexity of the considered DCO schemes at the Tx is given in Table II. The ACO schemes require twice more subcarriers compared to DCO schemes.

Figure 19 shows the complexity analysis in terms of the total number of arithmetic operations required at the Tx[11] for different ACO and DCO schemes considering a fixed data-rate R_b. As expected, the required number of arithmetic operations increases with increased number of data-carrying symbols $\mathcal{M}$. O-ROFDMA and O-SCFDMA have, respectively, the lowest

---

[11]Note that we focus on the Tx side, as it concerns the battery lifetime of the CN in the considered application.

and the highest complexity. Moreover, the number of arithmetic operations required by ACO-ROFDMA is equal to that for DCO-OFDMA.

VII. CONCLUSION

We proposed a HS-free O-ROFDMA scheme which transmits only the real part of the time-domain signal for the uplink extra-WBANs in an emergency waiting room scenario. We investigated the proposed scheme in terms of energy efficiency and computational complexity. More specifically, taking into account the parameters of realistic opto-electronic components, we studied the BER performance of DCO-ROFDMA and ACO-ROFDMA, compared with O-OFDMA and O-SCFDMA counterparts. In particular, we demonstrated the effect of induced MAI due to signal clipping, resulting in a loss of orthogonality between the signals of different users. Focusing then on ACO-ROFDMA as a more appropriate scheme due to its better energy efficiency (despite the requirement of a larger BW), we investigated the impact of MAI under fixed and randomly oriented Txs. We further showed that, thanks to the reduced computational complexity of O-ROFDMA, compared with O-OFDMA, a significant reduction in the Tx (CN) energy consumption can be achieved for medical WBANs.

As future research directions, it will be interesting to investigate the use of multiple AP arrangements for large-size indoor spaces, and to develop efficient solutions for time synchronization between the APs and hand-overs within a multi-cell architecture, in order to ensure high-fidelity medical data transmission under user mobility conditions.

REFERENCES

[1] P. K. Plunkett, D. G. Byrne, T. Breslin, K. Bennett, and B. Silke, "Increasing wait times predict increasing mortality for emergency medical admissions," *Eur. J. Emerg. Med.*, vol. 18, pp. 192–196, Aug. 2011.

[2] O. Haddad, M. A. Khalighi, S. Zvanovec, and M. Adel, "Channel characterization and modeling for optical wireless body-area networks," *IEEE Open J. Commun. Soc.*, vol. 1, pp. 760–776, 2020.

[3] S. Movassaghi, M. Abolhasan, J. Lipman, D. Smith, and A. Jamalipour, "Wireless body area networks: A survey," *IEEE Commun. Surveys Tuts.*, vol. 16, no. 3, pp. 1658–1686, 3rd Quart., 2014.

[4] B. Latré, B. Braem, I. Moerman, C. Blondia, and P. Demeester, "A survey on wireless body area networks," *Wireless Netw.*, vol. 17, no. 1, pp. 1–18, Jan. 2011.

[5] O. Haddad, M. A. Khalighi, and S. Zvanovec, "Channel characterization for optical extra-WBAN links considering local and global user mobility," in *Proc. Broadband Access Commun. Technol. XIV*, vol. 11307, 2020, pp. 89–97.

[6] M. J. Hasan, M. A. Khalighi, J. García-Márquez, and B. Béchadergue, "Performance analysis of optical-CDMA for uplink transmission in medical extra-WBANs," *IEEE Access*, vol. 8, pp. 171672–171685, 2020.

[7] Z. Ghassemlooy, L. N. Alves, S. Zvanovec, and M. A. Khalighi, *Visible Light Communications: Theory and Applications*. New York, NY, USA: CRC Press, 2017.

[8] M. Giordani, M. Polese, M. Mezzavilla, S. Rangan, and M. Zorzi, "Toward 6G networks: Use cases and technologies," *IEEE Commun. Mag.*, vol. 58, no. 3, pp. 55–61, Mar. 2020.

[9] O. Haddad and M. A. Khalighi, "Enabling communication technologies for medical wireless body-area networks," in *Proc. Global LiFi Congr. (GLC)*, Paris, France, Jun. 2019, pp. 1–5.

[10] T. B. Hoang, S. Sahuguède, and A. Julien-Vergonjanne, "Optical wireless network design for off-body-sensor based monitoring," *Wireless Commun. Mobile Comput.*, vol. 2019, p. 13, Sep. 2019.

[11] *Photobiological Safety of Lamps and Lamp Systems*, IEC Standard 62471, 2008.

[12] M. J. Hasan, M. A. Khalighi, and B. Bechadergue, "Experimental implementation of optical-CDMA for medical extra-WBAN links," in *Proc. 12th Int. Symp. Commun. Syst. Netw. Digit. Signal Process. (CSNDSP)*, Porto, Portugal, Jul. 2020, pp. 1–6.

[13] D. R. Dhatchayeny, S. Arya, and Y. H. Chung, "Infrared-based multiple-patient monitoring in indoor optical wireless healthcare systems," *IEEE Sensors J.*, vol. 19, no. 14, pp. 5594–5599, Jul. 2019.

[14] G. Sun, K. Wang, H. Yu, X. Du, and M. Guizani, "Priority-based medium access control for wireless body area networks with high-performance design," *IEEE Internet Things J.*, vol. 6, no. 3, pp. 5363–5375, Jun. 2019.

[15] J. An, N. Q. Pham, and W. Chung, "Multiple bio-monitoring system using visible light for electromagnetic-wave free indoor healthcare," *Opt. Commun.*, vol. 405, pp. 107–113, Dec. 2017.

[16] E. A. Alyan and S. A. Aljunid, "Development of wireless optical CDMA system for biosignal monitoring," *Optik*, vol. 145, pp. 250–257, Sep. 2017.

[17] J. An and W. Chung, "Single-LED multichannel optical transmission with SCMA for long range health information monitoring," *J. Lightw. Technol.*, vol. 36, no. 23, pp. 5470–5480, Dec. 1, 2018.

[18] Q. Wang, R. Zhang, L. Yang, and L. Hanzo, "Non-orthogonal multiple access: A unified perspective," *IEEE Wireless Commun.*, vol. 25, no. 2, pp. 10–16, Apr. 2018.

[19] C. Chen, S. Fu, X. Jian, M. Liu, X. Deng, and Z. Ding, "NOMA for energy-efficient LiFi-enabled bidirectional IoT communication," *IEEE Trans. Commun.*, vol. 69, no. 3, pp. 1693–1706, Mar. 2021.

[20] M. W. Eltokhey, M. Khalighi, and Z. Ghassemlooy, "Multiple access techniques for VLC in large space indoor scenarios: A comparative study," in *Proc. Int. Conf. Telecommun. (ConTEL)*, Jul. 2019, pp. 1–6.

[21] J. Ding, M. Nemati, C. Ranaweera, and J. Choi, "IoT connectivity technologies and applications: A survey," *IEEE Access*, vol. 8, pp. 67646–67673, 2020.

[22] M. Shirvanimoghaddam, M. Dohler, and S. J. Johnson, "Massive non-orthogonal multiple access for cellular IoT: Potentials and limitations," *IEEE Commun. Mag.*, vol. 55, no. 9, pp. 55–61, Sep. 2017.

[23] J. Armstrong, "OFDM for optical communications," *J. Lightw. Technol.*, vol. 27, no. 3, pp. 189–204, Feb. 1, 2009.

[24] T. Essalih, M. A. Khalighi, S. Hranilovic, and H. Akhouayri, "Optical OFDM for SiPM-based underwater optical wireless communication links," *Sensors*, vol. 20, no. 21, p. 6057, 2020.

[25] J. Armstrong and B. J. C. Schmidt, "Comparison of asymmetrically clipped optical OFDM and DC-biased optical OFDM in AWGN," *IEEE Commun. Lett.*, vol. 12, no. 5, pp. 343–345, May 2008.

[26] M. Khalighi, S. Long, S. Bourennane, and Z. Ghassemlooy, "PAM- and CAP-based transmission schemes for visible-light communications," *IEEE Access*, vol. 5, pp. 27002–27013, 2017.

[27] H. Qian, S. J. Yao, S. Z. Cai, and T. Zhou, "Adaptive postdistortion for nonlinear LEDs in visible light communications," *IEEE Photon. J.*, vol. 6, no. 4, pp. 1–8, Aug. 2014.

[28] H. Elgala, R. Mesleh, and H. Haas, "An LED model for intensity-modulated optical communication systems," *IEEE Photon. Technol. Lett.*, vol. 22, no. 11, pp. 835–837, Jun. 1, 2010.

[29] S. Long and M. A. Khalighi, "Advantage of CAP signaling for VLC systems under non-linear LED characteristics," in *Proc. West Asian Colloq. Opt. Wireless Commun. (WACOWC)*, Tehran, Iran, Apr. 2019, pp. 21–25.

[30] A. Anton, G. Martin, G. Onushkin, and J.-P. Linnartz, "Accurate thermal transient measurements interpretation of monochromatic LEDs," in *Proc. 35th Semicond. Thermal Meas. Model. Manage. Symp. (SEMI-THERM)*, San Jose, CA, USA, 2019, pp. 7–11.

[31] S. Dimitrov, S. Sinanovic, and H. Haas, "Clipping noise in OFDM-based optical wireless communication systems," *IEEE Trans. Commun.*, vol. 60, no. 4, pp. 1072–1081, Apr. 2012.

[32] W. Hu, "SLM-based ACO-OFDM VLC system with low-complexity minimum amplitude difference decoder," *Electron. Lett.*, vol. 54, no. 3, pp. 144–146, 2018.

[33] W. O. Popoola, Z. Ghassemlooy, and B. G. Stewart, "Pilot-assisted PAPR reduction technique for optical OFDM communication systems," *J. Lightw. Technol.*, vol. 32, no. 7, pp. 1374–1382, Apr. 1, 2014.

[34] S. S. Bawazir, P. C. Sofotasios, S. Muhaidat, Y. Al-Hammadi, and G. K. Karagiannidis, "Multiple access for visible light communications: Research challenges and future trends," *IEEE Access*, vol. 6, pp. 26167–26174, 2018.

[35] Y.-J. Chang, F.-T. Chien, and C.-C. J. Kuo, "Cross-layer QoS analysis of opportunistic OFDM-TDMA and OFDMA networks," *IEEE J. Sel. Areas Commun.*, vol. 25, no. 4, pp. 657–666, May 2007.

[36] A. W. Azim, Y. Le Guennec, and G. Maury, "Hermitian symmetry free optical-single-carrier frequency division multiple access for visible light communication," *Opt. Commun.*, vol. 415, pp. 177–185, May 2018.

[37] H. G. Myung and D. J. Goodman, *Single Carrier FDMA*. Chichester, U.K.: Wiley, 2008, pp. 37–59.

[38] V. Jungnickel and L. Grobe, "Localized SC-FDMA with constant envelope," in *Proc. IEEE Int. Symp. Pers. Indoor Mobile Radio Commun. (PIMRC)*, Sep. 2013, pp. 24–29.

[39] R. G. A. Gallo, A. M. Abdelaziz, M. Alghoniemy, and H. M. H. Shalaby, "Real-DFT based DCO-OFDM and ACO-OFDM for optical communications systems," in *Proc. Int. Conf. Transp. Opt. Netw. (ICTON)*, Jul. 2019, pp. 1–4.

[40] J.-P. M. G. Linnartz and X. Deng, "Continuous phase Flip-OFDM in optical wireless communications," *Signal Process.*, vol. 182, May 2021, Art. no. 107963.

[41] C. Chen, D. A. Basnayaka, and H. Haas, "Downlink performance of optical attocell networks," *J. Lightw. Technol.*, vol. 34, no. 1, pp. 137–156, Jan. 1, 2016.

[42] M. W. Eltokhey, M. A. Khalighi, A. S. Ghazy, and S. Hranilovic, "Hybrid NOMA and ZF pre-coding transmission for multi-cell VLC networks," *IEEE Open J. Commun. Soc.*, vol. 1, pp. 513–526, 2020.

[43] R. Cavallari, F. Martelli, R. Rosini, C. Buratti, and R. Verdone, "A survey on wireless body area networks: Technologies and design challenges," *IEEE Commun. Surveys Tuts.*, vol. 16, no. 3, pp. 1635–1657, 3rd Quart., 2014.

[44] M. Patel and J. Wang, "Applications, challenges, and prospective in emerging body area networking technologies," *IEEE Wireless Commun.*, vol. 17, no. 1, pp. 80–88, Feb. 2010.

[45] L. Chevalier, S. Sahuguède, and A. Julien-Vergonjanne, "Optical wireless links as an alternative to radio-frequency for medical body area networks," *IEEE J. Sel. Areas Commun.*, vol. 33, no. 9, pp. 2002–2010, Sep. 2015.

[46] *HDN1102W-TR Standard Product Specifications*, Stanley Electr., Tokyo, Japan, 2014.

[47] V. Jungnickel *et al.*, "Demonstration of virtual MIMO in the uplink," in *Proc. IET Smart Antennas Cooper. Commun. Seminar*, London, U.K., 2007, pp. 1–7.

[48] M. Morelli, L. Sanguinetti, and H. V. Poor, "A robust ranging scheme for OFDMA-based networks," *IEEE Trans. Commun.*, vol. 57, no. 8, pp. 2441–2452, Aug. 2009.

[49] Y. Jiang, Y. Wang, P. Cao, M. Safari, J. Thompson, and H. Haas, "Robust and low-complexity timing synchronization for DCO-OFDM LiFi systems," *IEEE J. Sel. Areas Commun.*, vol. 36, no. 1, pp. 53–65, Jan. 2018.

[50] S. Tian, K. Panta, H. A. Suraweera, B. J. C. Schmidt, S. McLaughlin, and J. Armstrong, "A novel timing synchronization method for ACO-OFDM-based optical wireless communications," *IEEE Trans. Wireless Commun.*, vol. 7, no. 12, pp. 4958–4967, Dec. 2008.

[51] T.-A. Truong, M. Arzel, H. Lin, B. Jahan, and M. Jezequel, "New low-complexity and robust time synchronization technique for optical IMDD OFDM transmissions," *Opt. Exp.*, vol. 22, no. 12, pp. 14322–14340, 2014.

[52] X. Qian, Y. Deng, H. Deng, Y. Hu, C. Zhang, and J. Du, "Synchronisation algorithm based on zero correlation code pair for OFDM-based VLC systems," *IET Commun.*, vol. 11, no. 2, pp. 205–210, 2017.

[53] J. M. Kahn and J. R. Barry, "Wireless infrared communications," *Proc. IEEE*, vol. 85, no. 2, pp. 265–298, Feb. 1997.

[54] F. Xu, M. Khalighi, and S. Bourennane, "Impact of different noise sources on the performance of PIN- and APD-based FSO receivers," in *Proc. 11th Int. Conf. Telecommun. (CONTEL)*, Jun. 2011, pp. 211–218.

[55] S. D. Dissanayake and J. Armstrong, "Comparison of ACO-OFDM, DCO-OFDM and ADO-OFDM in IM/DD systems," *J. Lightw. Technol.*, vol. 31, no. 7, pp. 1063–1072, Apr. 1, 2013.

[56] A. V. Oppenheim and R. W. Schafer, *Discrete-Time Signal Processing*, 3rd ed. Upper Saddler River, NJ, USA: Prentice Hall Press, 2009.

[57] S. So and K. K. Paliwal, "Reconstruction of a signal from the real part of its discrete fourier transform [tips & tricks]," *IEEE Signal Process. Mag.*, vol. 35, no. 2, pp. 162–174, Mar. 2018.

[58] H. Elgala, R. Mesleh, and H. Haas, "Non-linearity effects and predistortion in optical OFDM wireless transmission using LEDs," *Int. J. Ultra Wideband Commun. Syst.*, vol. 1, no. 2, pp. 143–150, 2009.

[59] C. Wu, H. Zhang, and W. Xu, "On visible light communication using LED array with DFT-spread OFDM," in *Proc. IEEE Int. Conf. Commun. (ICC)*, Aug. 2014, pp. 3325–3330.

[60] S. H. Han and J. H. Lee, "An overview of peak-to-average power ratio reduction techniques for multicarrier transmission," *IEEE Wireless Commun.*, vol. 12, no. 2, pp. 56–65, Apr. 2005.

[61] J. Armstrong and A. Lowery, "Power efficient optical OFDM," *Electron. Lett.*, vol. 42, pp. 370–372, Mar. 2006.

[62] V. Jungnickel, T. Hindelang, T. Haustein, and W. Zirwas, "SC-FDMA waveform design, performance, power dynamics and evolution to MIMO," in *Proc. IEEE Int. Conf. Portable Inf. Devices*, May 2007, pp. 1–6.

[63] W. Zheng, K. Li, and K. Li, "Scaled radix-2/8 algorithm for efficient computation of length-$N = 2^m$ DFTs," *IEEE Trans. Signal Process.*, vol. 62, no. 10, pp. 2492–2503, Mar. 2014.

[64] J. Cooley and J. Tukey, "An algorithm for the machine calculation of complex Fourier series," *Math. Comput.*, vol. 19, no. 90, pp. 297–301, 1965.

Md. Jahid Hasan (Member, IEEE) received the Ph.D. degree for his work on multi-user data transmission in optical wireless body area networks for medical applications from the École Centrale de Marseille, France, in 2021, and the joint international M.Sc. degree in smart systems integration from Heriot-Watt-University, Edinburgh, U.K., in 2016. His Ph.D. thesis work was funded by the European Union's Marie Sklodowska-Curie Vision ITN Project. He is currently serving as an Assistant Professor with the Department of Electrical and Electronic Engineering (EEE), American International University-Bangladesh (AIUB), Dhaka, Bangladesh. From 2012 to 2014, he worked as an ASIC Design Engineer with Fastrack Anontex Ltd., Dhaka. He also served as a Lecturer with the Department of EEE, AIUB from 2017 to 2018. From 2018 to 2021, he worked as an Early-Stage Researcher with the Vision ITN Project hosted by Oledcomm SAS, Paris, France. His research interests include optical wireless communications, digital signal processing, and FPGA-based implementation. He was also a recipient of the Erasmus Mundus scholarship during his two years M.Sc. Program from 2014 to 2016.

Mohammad Ali Khalighi (Senior Member, IEEE) is an Associate Professor with École Centrale Marseille, Marseille, France, and the Head of Optical Communications for IoT Group, Fresnel Institute Research Lab. His main research interests include wireless communication systems with an emphasis on free-space, underwater, and visible-light optical communications. He is currently serving as the Action Chair for the COST Action CA19111 NEWFOCUS (European Network on Future Generation Optical Wireless Communication Technologies). He was the Coordinator of the H2020 ITN MSCA VisIoN Project (Visible-Lightbased Interoperability and Networking). He is also serving as the Editor-at-Large for the IEEE TRANSACTIONS ON COMMUNICATIONS, and has served as an Associate Editor for the *Electronics Letters* as well as a Lead Guest Editor for the IEEE OPEN JOURNAL OF THE COMMUNICATIONS SOCIETY.

Volker Jungnickel (Member, IEEE) received the Ph.D. degree in physics in 1995 and the Habilitation degree in communications engineering in 2015. He joined Fraunhofer HHI in 1997, working on optical wireless communications, multiple antennas in mobile networks, and fixed optical access networks. He teaches and supervises thesis with TU Berlin, where he was appointed as an Extraordinary Professor in 2021. He serves in optical wireless standards as a Chair of IEEE P802.15.13 and as a Technical Editor of IEEE P802.11bb.

Luis Nero Alves (Member, IEEE) received the graduate and M.Sc. degrees in electronics and telecommunication engineering from the University of Aveiro in 1996 and 2000, respectively, and the Ph.D. degree in electrical engineering from the University of Aveiro in 2008. His Ph.D. thesis was on high bandwidth gain product amplifiers for optical wireless applications. He is currently with the Department of Electronics Telecommunications and Informatics from the University of Aveiro, where he lectures electronic related subjects to both graduate and undergraduate students. Since 2008, he has been the Lead Researcher with the Integrated Circuits Group from the Instituto de Telecomunicações–Aveiro. He has authored/coauthored several conference and journal papers on the aforementioned topics. His current research interests are on: 1) design and performance analysis of visible light communications systems; 2) visible light communications systems applied to IoT scenarios; 3) IoT sensing devices, especially focused on SAW (surface acoustic wave) and memristive devices; 4) sensing and stimulation devices for implantable medical devices; and 5) analogue integrated circuit design for sensing and instrumentation applications. He has participated in the technical program committee of several international conferences on optical communications. He has served as a Reviewer for several international journals IEEE PHOTONICS TECHNOLOGY LETTERS, *Journal of Lightwave Technology*, IEEE TRANSACTIONS ON CIRCUITS AND SYSTEMS—I: REGULAR PAPERS, IEEE TRANSACTIONS ON CIRCUITS AND SYSTEMS—II: EXPRESS BRIEFS, IEEE TRANSACTIONS ON CIRCUITS AND SYSTEMS FOR VIDEO TECHNOLOGY, and *Optics Communications* (Elsevier). He has served as a member of the COST actions IC1401 (MemoCiS), IC1101 (OPTICWISE), and CA19111 (NEWFOCUS). He has participated/leaded several research projects at both national and international levels, such as, NeuralStimSpinal (H2020/FET), VisIoN (H2020/MSCA-ITN), LITES (EU/CIP-ICT-PSP) SGH (P2020/SI I&DT), RTMGear (FP7/CleanSky), and VLCLighting (IT/Internal).

Bastien Béchadergue received the Aeronautical Engineering degree from ISAESupaero, Toulouse, France, the M.Sc. degree in communication and signal processing from Imperial College London, London, U.K., in 2014, and the Ph.D. degree in signal and image processing from UVSQ, Université Paris-Saclay, France, in 2017, for his work on visible light communication and sensing for automotive applications. From 2017 and 2020, he was an In-Charge of the research activities with Oledcomm, one of the leading companies in the development of optical wireless communication products. Since 2020, he has been an Associate Professor with UVSQ, Université Paris-Saclay, where his research focuses on optical wireless communication and sensing.